Journal of Intelligent Systems and Control
https://www.acadlore.com/journals/JISC

Robust Speed Control in Nonlinear Electric Vehicles Using H-Infinity Control and the LMI Approach

Farid Oudjama[1*], Abdelmadjid Boumediene[1], Khayreddine Saidi[1,2*], Djamila Boubekeur[3,4]

[1] LAT, Laboratoire d'Automatique de Tlemcen, Tlemcen University, 13000 Tlemcen, Algeria
[2] Electrical Engineering faculty, Djillali Liabes University, 22000 Sidi Bel Abbes, Algeria
[3] MELT, Manufacturing Engineering Laboratory of Tlemcen, Tlemcen University, 13000 Tlemcen, Algeria
[4] Institut des Sciences et Techniques Appliquées, Université Oran1, 31000 Oran, Algeria

[*] Correspondence: Khayreddine Saidi (saidi_kheiro@yahoo.fr); Farid Oudjama (faridoudjama@gmail.com)

Received: 08-11-2023 **Revised:** 09-10-2023 **Accepted:** 09-18-2023

Citation: F. Oudjama, A. Boumediene, K. Saidi, and D. Boubekeur, "Robust speed control in nonlinear electric vehicles using H-infinity control and the LMI approach," *J. Intell Syst. Control*, vol. 2, no. 3, pp. 170–182, 2023. https://doi.org/10.56578/jisc020305.

Abstract: In this investigation, the robust H∞ control of nonlinear electric vehicles (EVs), powered by permanent magnet synchronous motors (PMSM), was examined. Emphasis was placed on enhancing the accuracy and robustness of the vehicle speed regulation by incorporating a meticulous H∞ method, supplemented by the proficient integration of Linear Matrix Inequality (LMI). A solution predicated on the LMI approach was devised, encompassing two distinct H∞ controllers for both current and speed control. Subsequent to an extensive analysis of the mathematical and control model of the EV, weighting functions were judiciously selected to optimize stability and performance. The proposed methodology offers significant advancements in the domain of EV control strategies and proffers insights into the application of robust control methods. Through comprehensive simulations, the effectiveness of the outlined method was validated, revealing impeccable speed control and ensuring steadfast performance when applied to the dynamic model of an EV equipped with a PMSM motor. This research elucidates the progressive strides made in the realm of EV control tactics and offers profound understandings of robust control methodologies.

Keywords: Electric vehicle (EV); Permanent magnet synchronous machine (PMSM); H-infinity robustness; Linear matrix inequality (LMI); Speed tracking

1 Introduction

Over the past several decades, challenges within control systems have been the focus of extensive research. Such challenges, including the introduction of undesirable variables like modeling uncertainty, the influence of measurement noise, and effects stemming from overlooked nonlinear dynamics, have necessitated the development of highly effective synthesis techniques. It has been observed that these techniques necessitate the synthesis of controllers which strike a balance between robust loop system stability and optimal performance [1]. Importantly, this balance is not merely restricted to the nominal operating speed of the system under control but also extends to numerous conditions wherein the synthetic model's parameters can exhibit significant variability.

Prominent among the applied robust methodologies, the H∞ control utilizing RICATTI equations and those leveraging the Linear Matrix Inequalities (LMI) approach have been cited [2–6]. It was in the early 1980s that this robust methodology found its origins, primarily attributed to the pioneering efforts of researchers like DOYLE and SAFONOV, wherein novel mathematical tools were introduced. Currently, this method stands as a primary research direction, particularly within the domain of robust techniques [2, 3, 5].

The central challenge identified in this study pertains to the development of more efficient control laws, especially concerning trajectory tracking, disturbance negation, stability, and robustness vis-a-vis parameter uncertainty [7, 8].

An EV, typically characterized by an electric motor operating exclusively on electrical energy, has at its core a PMSM. This motor, while bringing benefits like a substantial reduction in weight and volume for a specific output power (high power density), also offers increased efficiency and effective heat dissipation. However, challenges such as pitch disturbance, augmented torque, vibration, and noise serve as significant impediments, particularly impacting EV performance in road-speed contexts [9, 10].

For ensuring consistent vehicular speed without frequent adjustments, and considering the aforementioned challenges, the cruise control system was designed, primarily focusing on facilitating safety, comfort, and ease of drive for users. In this context, the robust H-infinity control, implemented via the LMI approach, was utilized for designing a controller specific to EVs powered by a PMSM [11]. Through this approach, stabilization and effective speed tracking were achieved.

Subsequent sections are structured as follows: Section 2 delves into the longitudinal mathematical model of EVs. Sections 3 and 4 focus on the design approach and its subsequent implementation for speed tracking control specific to EVs. Performance evaluations of the controller, facilitated by comprehensive numerical simulations, are presented in Section 5, with concluding remarks featured in Section 6.

2 Problem Description

As depicted in Figure 1, the dynamics of the EV system can be primarily segmented into two components: motor system dynamics and vehicle dynamics. The motor system is interfaced with the EV system through a transmission unit, encompassing the transmission system. In a standard EV setup, accelerator/brake pedals are employed by the driver to relay acceleration/deceleration command signals to the controller. A PMSM motor, which is integrated with the EV system through a transmission unit equipped with a gear system, is utilized to propel the aforementioned EV system. In essence, the speed of the PMSM motor is modulated to control the overall EV system [9, 12].

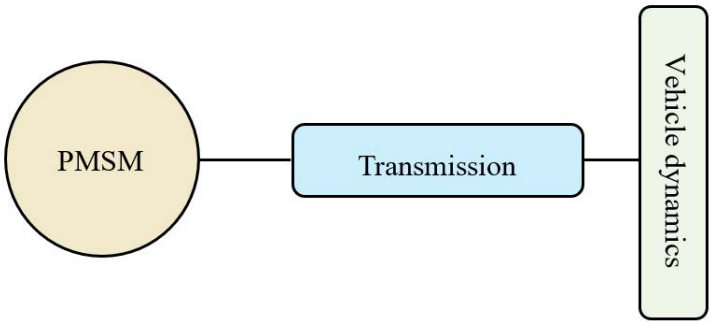

Figure 1. Configuration of the EV

2.1 Vehicle Dynamics Modeling

The dynamic model of the vehicle, based on the cumulative forces exerted upon it (refer to Figure 2), is governed by Newton's second law [9, 10, 13–16].

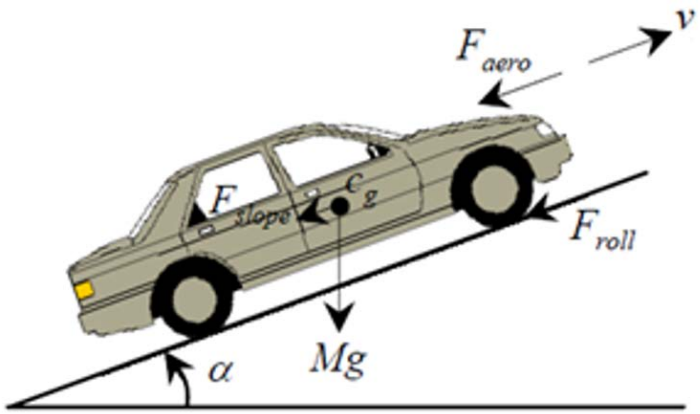

Figure 2. Applied forces on a vehicle

The summation of all active forces yields the total resultant force, given by:

$$F = Mgf_r\cos(\alpha) + \frac{1}{2}\rho A_f C_D V^2 + Mg\sin(\alpha) + M\frac{dV}{dt} \tag{1}$$

(1) The gravitational force, which acts upon a vehicle during incline traversal, is determined by the slope angle and is proportional to the vehicle's mass. It is represented as:

$$F_g = Mg\sin(\alpha) \tag{2}$$

(2) The aerodynamic resistance force, created by air flowing over the moving vehicle's body, is influenced by the vehicle's frontal area orientation. Its mathematical representation is:

$$F_{\text{aero}} = \frac{1}{2}\rho A_f C_D V^2 \tag{3}$$

(3) The primary source of rolling resistance arises from the friction between the vehicle's tires and the road surface, opposing the direction of vehicle movement. This force is defined by:

$$F_r = Mgf_r\cos(\alpha) \tag{4}$$

The resultant force, F, produced due to the friction between the vehicle tires and the road, generates a torque that impacts the drive motor. Termed as the traction force, it plays a pivotal role in vehicle propulsion and is expressed as:

$$T_L = F \times \frac{R_{\text{wheel}}}{K_{\text{gear}}} \tag{5}$$

The association between the motor's angular velocity, Ω_{mot}, and the EV's linear speed, V, is elucidated as:

$$V = \frac{R_{\text{wheel}}}{K_{\text{gear}}}\Omega_{\text{mot}} \tag{6}$$

where, T_L is the torque generated by the driving motor, R_{wheel} is the wheel radius, and Ω_{mot} is the rotation speed of the motor.

• Gearbox

The inclusion of a gearbox in an EV is noted to augment engine efficiency by modulating the relationship between engine velocity and wheel speed. Such modulation of torque in alignment with driving conditions contributes to an enhanced driving range and experience. The mechanical conversion value is procured from the ensuing equation [17, 18]:

$$\begin{cases} T_{\text{gear}} = K_{\text{gear}} \times T_{\text{mot}} \\ \Omega_{\text{mot}} = K_{\text{gear}} \times \Omega_{\text{gear}} \end{cases} \tag{7}$$

where, T_{gear} and Ω_{gear} are torque and speed rotation after reduction, Ω_{mot} is the motor rotation speed and K_{gear} is the gearbox reduction coefficient.

• Differential mechanical

The mechanical differential in EVs is imperative for power distribution between wheels, ensuring optimal traction and stability. Moreover, it modulates wheel rotation speeds during turns to prevent skidding. The even torque distribution to both the left and right wheels is depicted in Eq. (8) [17, 18]:

$$\begin{cases} T_{\text{diff left}} = \frac{1}{2}T_{\text{gear}} \\ T_{\text{diff right}} = \frac{1}{2}T_{\text{gear}} \\ T_{\text{diff Tot}} = T_{\text{diff right}} + T_{\text{diff}_{\text{left}}} \end{cases} \tag{8}$$

where, $T_{\text{diff left}}$, $T_{\text{diff right}}$ and $T_{\text{diff Tot}}$ are left, right and total torques after differential, respectively.

• The traction forces

Using wheel rotation, differential torque, and vehicle speed, the traction forces can be calculated:

$$\begin{cases} F_{\text{left}} = \frac{1}{R_{\text{wheel}}}T_{\text{diff left}} \\ W_{\text{left}} = \frac{1}{R_{\text{wheel}}}V_{\text{veh left}} \\ F_{\text{right}} = \frac{1}{R_{\text{wheel}}}T_{\text{diff right}} \\ W_{\text{right}} = \frac{1}{R_{\text{wheel}}}V_{\text{veh right}} \end{cases} \tag{9}$$

where, R_{wheel} is the wheel radius, $T_{\text{diff right}}$ and $T_{\text{diff } Tot}$ are left, right and total torques after differential, respectively.

2.2 Model of the Traction Motor

The representation of the equations describing the PMSM model is situated in the rotor frame (d-q) [19–21]. The subsequent equations can be derived:

$$\begin{cases} \frac{di_d}{dt} = -\frac{R_s}{L} i_d + P_p i_q + \frac{1}{L} u_d \\ \frac{di_q}{dt} = -\frac{R_s}{L} i_q - P_p \Omega_{mot} i_d - \frac{P_p \Phi}{L} \Omega_{mot} + \frac{1}{L} u_q \\ \frac{d\Omega_{mot}}{dt} = \frac{3 P_p \Phi}{2J} i_q - \frac{B}{J} \Omega_{mot} + \frac{T_L}{J} \end{cases} \tag{10}$$

where, the terms u_d, u_q, i_d and i_q are defined as stator voltages and currents in the d-q frame respectively. R_s signifies the stator resistance, while L denotes the inductance in the d-q frame. P_p stands for the pole pairs and Φ is the permanent magnet flux. J represents the rotor moment of inertia, B is the viscous friction coefficient, and T_L is the load torque.

By incorporating Eq. (1), Eq. (5), and Eq. (6) into Eq. (10), the dynamic model of the entire EV system is defined. This integration combines the PMSM model with the vehicle dynamics model, given by:
with $J_v = \frac{J K_{\text{gear}}{}^2 + M R_{\text{wheel}}{}^2}{R_{\text{wheel}} K_{\text{gear}}}$. The state vector x assumes the forms of $x = [x_1, x_2, x_3]^T = [i_d, i_q, V]^T$.

From Eq. (10), it can be discerned that the model is nonlinear. However, for effective tracking of the desired vehicle speed with the robust H∞ controller, a linear model is imperative. To mitigate this challenge, non-linear effects, such as friction, were neglected, and a compensation method that simplifies torque control was applied. This approach involved the linearization of the relationship between torque and current, thus establishing a linear and single-input model for the permanent magnet synchronous machine.

Subsequent computations yielded the transfer functions for the d-axis current and the speed system:

$$G_{id} = \frac{1}{R_s + sL} \tag{11}$$

$$G_V = \frac{3 P_p \Phi K_{\text{gear}}}{(J_v R_{\text{wheel}}\, s + B K_{\text{gear}})\,(Ls + R_s) + 3 P_p^2 \Phi^2 K_{\text{gear}}{}^2} \tag{12}$$

3 H∞ Control Analysis

H∞ techniques have been recognized as robust control approaches, prominently designed to bolster stability while optimizing performance. Their significance, particularly within dynamic systems such as EV speed control, cannot be overstressed [22, 23].

LMI techniques were employed in the design of the H∞ suboptimal controllers. Within the paradigm of H∞ control design, the LMI strategy was adopted to discern controller gains, ensuring the stability of the closed-loop system and concurrently minimizing a defined H∞ norm from disturbance input to the output signal. The efficacy of the LMI technique in transforming the H∞ control issue into a LMI set was substantiated through numerical methods [11, 21, 24].

A schematic representation incorporating the envisaged H∞ controller can be discerned in Figure 3 [2, 3, 5, 25]. Within this configuration:

- P(s) typifies the generalized plant.
- K(s) delineates the controller.
- Variables ω, Z, y and u represent exogenous inputs, minimized output signals, measurement outputs, and control signals, respectively.

Figure 3. H∞ control framework

Generalized plant $P(s)$ encompasses the plant model $G(s)$, the interconnection structure, and the weighting functions predetermined by the designer, formulated as:

$$\begin{bmatrix} \dot{x}(t) \\ e(t) \\ y(t) \end{bmatrix} = \begin{bmatrix} A & B_1 & B_2 \\ C_1 & D_{11} & D_{12} \\ C_2 & D_{21} & D_{22} \end{bmatrix} \begin{bmatrix} x(t) \\ \omega(t) \\ u(t) \end{bmatrix} \tag{13}$$

Given the variables $x \in \Re^n$, $\omega \in \Re^{n_\omega}$, $u \in \Re^{n_u}$, $e \in \Re^{n_e}$, $y \in \Re^{n_y}$, the system's stabilizability of (A, B_2) and the detectability of (C_2, A) were taken into account. The transfer matrix in a closed loop from ω to the performance output Z is articulated as:

$$H_{zw}(s) = C_c \left(sI - A_c\right)^{-1} B_c + D_c \tag{14}$$

The crux of the H∞ control issue lies in identifying a controller that ensures the H∞ norm of the $H_{zw}(s)$ transfer function remains below γ. The bounded lemma, integral to the H∞ evaluation, establishes that the H∞ norm of $H_{zw}(s)$ is less than γ if, and only if, a positive definitive matrix $\mathbb{P}$ meets the prescribed criteria.

$$\begin{bmatrix} A_c^T\mathbb{P} + \mathbb{P}A_c & \mathbb{P}B_c & C_c^T \\ B_c^T\mathbb{P} & -\gamma I & D_c^T \\ C_c & D_c & -\gamma I \end{bmatrix} < 0$$

The solvability of the H∞ control dilemma is contingent upon the existence of symmetric matrices R, S that satisfy the prescribed LMI system [11, 21, 24, 25]:

(1) LMI

$$\begin{pmatrix} N_X^T & 0 \\ 0 & I \end{pmatrix}^T \begin{pmatrix} AX + XA^T & XC_1^T & B_1 \\ C_1X & -\gamma I & D_{11} \\ B_1^T & D_{11}^T & -\gamma I \end{pmatrix} \begin{pmatrix} N_X & 0 \\ 0 & I \end{pmatrix} < 0 \tag{15}$$

Has a positive definite solution X.

(2) LMI

$$\begin{bmatrix} N_Y^T & 0 \\ 0 & I \end{bmatrix} \begin{pmatrix} YA + A^TY & YB_1 & C_1^T \\ B_1^TY & -\gamma I & D_{11}^T \\ C_1 & D_{11} & -\gamma I \end{pmatrix} \begin{pmatrix} N_Y & 0 \\ 0 & I \end{pmatrix} < 0 \tag{16}$$

Has a positive definite solution Y.

(3) Moreover, X and Y are bound by specific conditions.

$$\begin{gathered} \begin{pmatrix} X & I \\ I & Y \end{pmatrix} \geq 0, \operatorname{rank}\begin{pmatrix} X & I \\ I & Y \end{pmatrix} \leq n_K + n \\ \operatorname{rank}\begin{pmatrix} X & I \\ I & Y \end{pmatrix} \leq n + r \Leftrightarrow \operatorname{rank}(I - XY) \leq r \end{gathered} \tag{17}$$

In which n_K is the degree of controller $K(s)$.

Where N_X and N_Y respectively represents bases of the null spaces of $\begin{pmatrix} B_2^T & D_{12}^T \end{pmatrix}$ $\begin{pmatrix} B_2^T, & D_{\text{inf2}}^T \end{pmatrix}$ and $\begin{pmatrix} C_2 & D_{21} \end{pmatrix}(C_2, D_{01})$.

In crafting a suboptimal controller, two pivotal steps were followed [26]. Firstly, the aforementioned triad of LMIs was resolved. Then, using the identified matrices R and S in conjunction with the plant state-space data, the controller was calculated.

Consequently, a stabilizing suboptimal controller was realized that ensures $\|H_{zw}(s)\|_\infty \leq \gamma$. By streamlining the controller LMI formula and adhering to stipulated assumptions, a suboptimal controller was derived [26]. This controller can be expressed as:

$$K = \begin{bmatrix} A_k & B_k \\ C_k & D_k \end{bmatrix} \tag{18}$$

where,

$A_k = A + \gamma^{-2}B_1B_1^TX_\infty - B_2B_2^TX_\infty - \left(I - \gamma^{-2}Y_\infty X_\infty\right)^{-1} Y_\infty C_2^TC_2$

$B_k = \left(I - \gamma^{-2}Y_\infty X_\infty\right)^{-1} Y_\infty C_2^T$

$C_k = -B_2^TX_\infty$

It is noteworthy that the derivation of the H∞ controller can be efficiently executed utilizing Matlab's LMI toolbox.

4 Application

In Figure 4, the overarching structure of the nonlinear EV drive system, predicated on the permanents magnets synchronous motor (PMSM), is illustrated. The motor's control strategy, which was investigated in this study, is also highlighted therein.

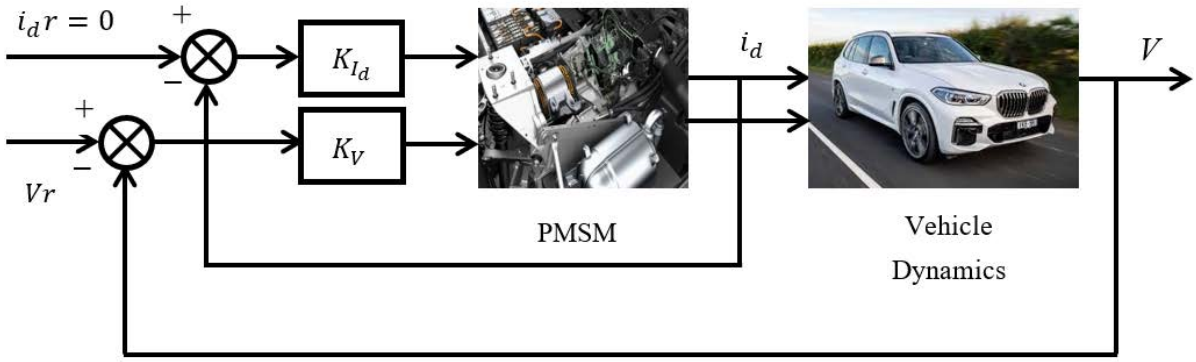

Figure 4. Block diagram of the proposed controller

The synthesis of controller design commenced with the selection of weight functions, as depicted in Figure 5 [7, 27, 28]. A paramount challenge associated with H∞ control pertains to the proper frequency-based selection of transfer functions and the order of weighting. It is understood that these weighting functions serve the purpose of defining system performance prerequisites, disturbance impacts, actuator boundaries, and system uncertainties.

Two distinctive loops can be discerned within the proposed control schema:

• The stator direct current control loop focuses on flux control. This loop is governed by an H∞ regulator. Through this regulator, the system's nonlinearity is sought to be negated by maintaining the direct current id at a null value.

• Another loop, managed by an H∞ regulator, is dedicated to speed control, specifically overseeing the speed and torque.

With the operation of the PMSM being under the purview of field-oriented control, its modeling, analogous to a DC motor, is evident.

4.1 Speed Loop Controller

Figure 5 delineates the speed loop block diagram encompassing weighting filters. Notably, the weight functions, symbolized as $W_{1V}(s)$, $W_{2V}(s)$, $W_{3V}(s)$, play a pivotal role in fine-tuning the controller's performance and robustness. Such functions can either represent a gain or be frequency-dependent.

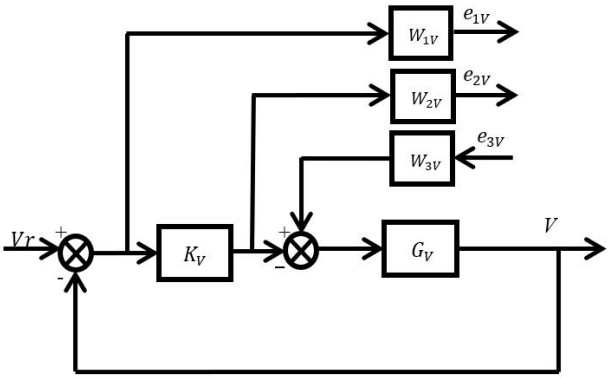

Figure 5. H∞ for the speed loop with weighting filters

Adherence to the foundational precepts of mixed design is witnessed in the weighting functions W_1, W_2 and W_3. Given that W_1 pertains to the objective of error sensitivity function performance S, it is fundamentally designed as a low pass filter to diminish error sensitivity in lower range frequencies for mitigating output disturbances. Conversely,

W_2 is integral for ascertaining the controlled system's stability across varying operations, rendering it as a high-pass filter. An auxiliary disturbance weighting function, W_3, delineates the disturbance limits, allowing it to be chosen as a high pass filter or retained as a constant.

For the issue at hand, which is speed control, the selected weighting functions aimed at crafting a controller that adheres to stipulated specifications (pertaining to tracking performance, anti-disturbance properties, and robustness) are defined as:

$$\begin{cases} W_{1V}(s) = \frac{0.5556s+500}{s+0.005} \\ W_{2V}(s) = \frac{1.378\times10^{-7}s+6.2\times10^{-5}}{0.001538s+1} \\ W_{3V}(s) = 0.01 \end{cases} \tag{19}$$

Upon utilizing the design showcased in Figure 5, the $K_V(s)$ controller can be derived by addressing the H-infinity problem via the LMI method. The ensuing expression for the controller is:

$K_V(s) = \frac{5.373\times10^8 s^3+3.646\times10^{11}s^2+1.028\times10^{13}s+1.862\times10^{14}}{s^4+53970s^3+3970s^2+1.067\times10^8 s+4.759\times10^{10}s+2.38\times10^8}$

4.2 Current Loop Controller

As Figure 6 demonstrates, the synthesis of the direct current loop controller uses weighting functions that are reminiscent of those in speed tracking synthesis. These functions are formulated as:

$$\begin{cases} W_{1i}(s) = \frac{0.5556s+500}{s+0.005} \\ W_{2i}(s) = \frac{0.0001375s+0.825}{0.001538s+1} \\ W_{3i}(s) = 0.01 \end{cases} \tag{20}$$

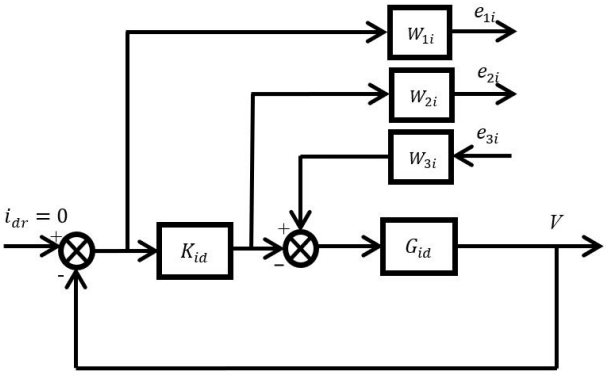

Figure 6. H∞ for the current loop with weighting filters

The H-infinity controller, represented by $K_I(s)$ for the current loop, takes the form:

$K_{id}(s) = \frac{1.027\times10^6 s^2+7.244\times10^9 s+3.698\times10^{12}}{s^3+1.019\times10^6 s^2+6.382\times10^9 s+3.191\times10^7}$

5 Simulation Results

To assess the perturbation rejection capabilities of the proposed H∞ controller, simulations were performed on an EV, utilizing the PMSM and EV parameters outlined in Table 1 and Table 2.

Initiating from a static state, the vehicle was observed to steadily accelerate to a reference speed of 80 km/h. Within this phase, two directional changes were enacted: the initial leftward shift occurred at t = 38.89 s, followed by a rightward shift at t = 83.33s. A return to the original trajectory was recorded at t = 111.11s, as visualized in Figure 7. Throughout these tests, the evolution of several electrical and mechanical variables, including currents, voltages, torque, and velocity, was monitored.

The results presented in Figure 8 depict the longitudinal speed of the vehicle. It was evident that the vehicle's speed remained stable, illustrating an agile performance devoid of overshoot, with no persistent errors identified. Notably, the system consistently matched the reference signal with remarkable precision.

During the turning phases, it was observed in Figure 9 that each wheel responded differently, rotating at varying speeds in the same direction. The H∞ controller's critical role was apparent, as it facilitated precise, real-time adjustments to the motor during these maneuvers, ensuring vehicular stability. Concurrently, a mechanical differential was engaged to equilibrate the speed disparity between wheels. This mechanism slowed the inner

Table 1. Parameters of the selected PMSM

The Parameter	Symbol	Value	Unit
d-axis Inductances	L_d	0.17	mH
q-axis Inductances	L_q	0.29	mH
Flux linkage	Φ	0.071	wb
Stator-winding resistance	R_s	0.0083	Ω
Number of poles	P_p	8	
Moment of inertia	J	0.089	$\mathrm{Kg} \cdot \mathrm{m}^2$
Moment of inertia	B	0.005	$\mathrm{Nm/rad/s}$

Table 2. Specifications of the vehicle used in the simulations

The Parameter	Symbol	Value	Unit
The mass of the vehicle	M	1450	Kg
Vehicle frontal area	A_f	2.711	m^2
Wheel radius	R_{wheel}	0.29	m
Aerodynamic drag coefficient	C_D	0.29	$\mathrm{Kg/m}^3$
Air density	ρ	1.204	
Rolling resistance coefficient	f_r	0.013	$\mathrm{Kg} \cdot \mathrm{m}^2$
Total inertia		5.209	
Total gear ratio	K_{gear}	8.75	

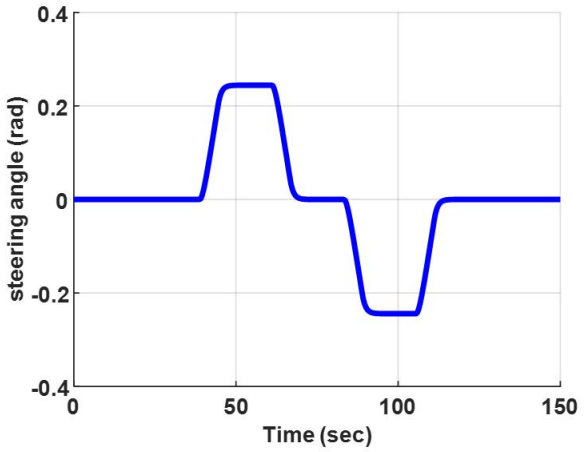

Figure 7. Steering angle representation

wheel, allowing the exterior wheel to rotate more rapidly, thus preventing skidding and control loss. This combined strategy enhanced traction, stability, and overall vehicle performance during turns. Evidently, the robust H∞ control mechanism presented superior tracking and control capabilities.

Figure 10 reveals the d-axis current response of the PMSM under two distinct control methods. Rapid alignment of the d-axis current response with the reference was noted across all trajectories.

The q-axis current responses and the electromagnetic torque of the PMSM in the vehicle system were highlighted in Figure 11 and Figure 12. The q-axis current component, proportional to the requisite torque, exhibited outstanding dynamic response. The required electromagnetic torque was efficiently developed by the PMSM motor at different speed reference stages, emphasizing the efficacy of the H∞ technique in PMSM control systems.

Figure 13 and Figure 14 present the phase voltages and phase currents throughout the operation. Both were observed to maintain a sinusoidal pattern, with frequency alterations in response to speed fluctuations.

Lastly, Figure 15 demonstrates the tractive forces exerted by the wheels. Strong tractive forces were observed initially, a necessary condition to overcome resistive forces opposing vehicle movement. Notably, a disparity in tractive forces was registered during the vehicle's navigations through turns, signifying the requirement for varied traction levels to facilitate efficient vehicle maneuvering during trajectory shifts.

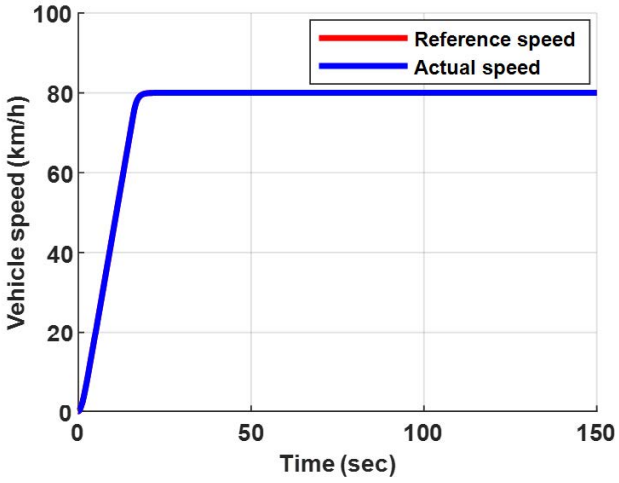

Figure 8. Vehicle's linear speed

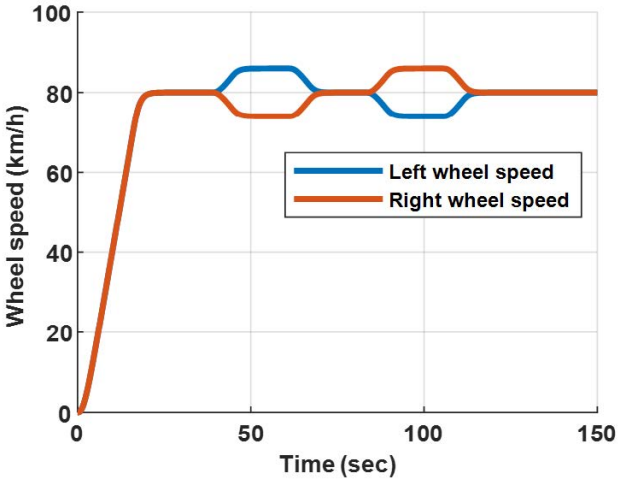

Figure 9. Speed variations during left and right turns

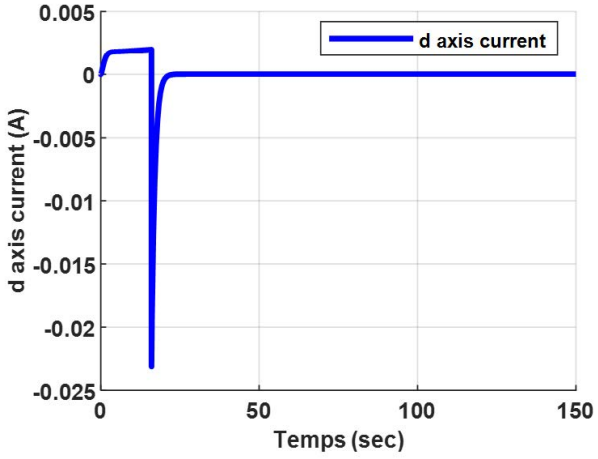

Figure 10. I_d-axis current

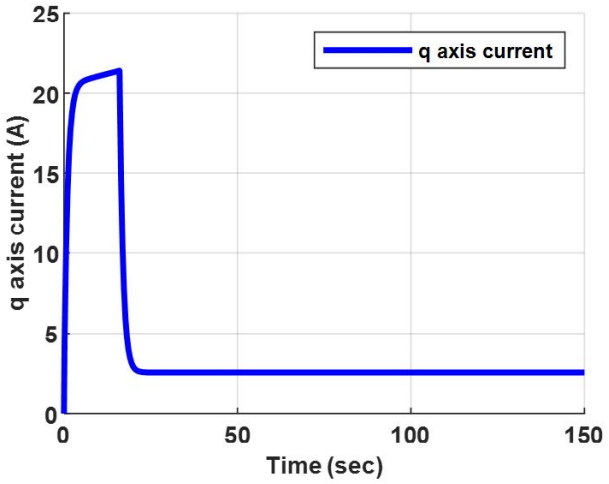

Figure 11. I_q-axis current

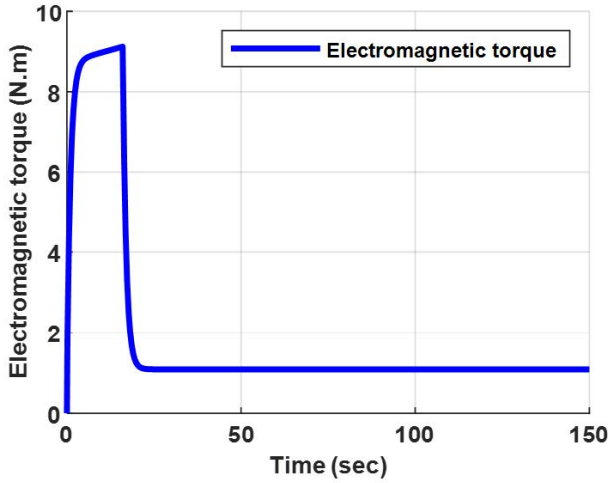

Figure 12. Electromagnetic torque

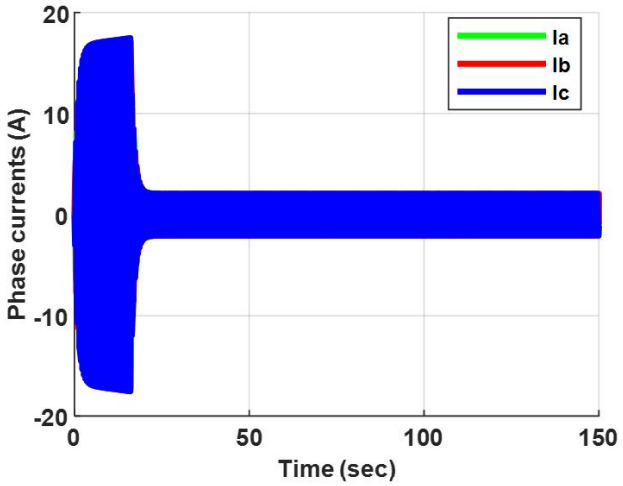

Figure 13. Phase currents of the motor

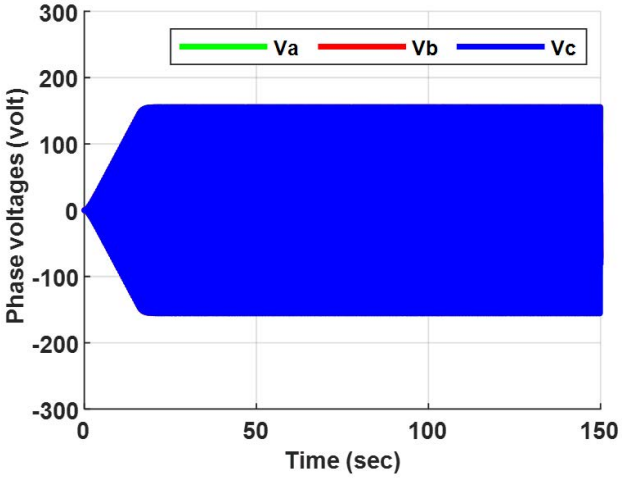

Figure 14. Phase voltages of the motor

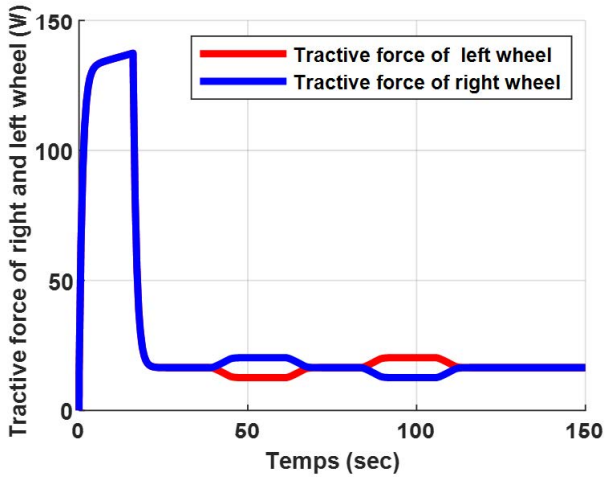

Figure 15. Tractive force generated by the wheels

6 Conclusions

In this investigation, an LMI-based solution for robust H∞ control of a nonlinear EV model powered by a PMSM was elucidated. The primary objective of this study was identified as the mitigation of interference effects, aiming to enhance the overall system performance.

Distinctively, the focus was on the peculiar attributes of EVs equipped with PMSM using robust H∞ control. The integration of control methodologies tailored for non-linearities, in conjunction with linear matrix inequalities, was found to be more adeptly matched to the demands of EVs than traditional techniques.

Within the proposed methodology, two H∞ controllers were employed: the first was identified as pivotal for the Id current loop control, and the second was crucial for precise speed regulation. Through the application of the vector control technique and judicious selection of weight functions, the stability and performance of the comprehensive system were observed to be enhanced.

The robust H∞ controller's efficacy was assessed through simulations utilizing a longitudinal model of the EV. The outcomes depicted superior dynamic and steady-state performances, thereby indicating the controller's competency in managing disturbances and ensuring meticulous velocity control.

The adoption of LMI-based synthesis for robust H∞ control in EVs revealed multiple benefits, encompassing augmented performance, stability, and robustness. Such findings suggest this method holds promise in refining EV control tactics, presenting a viable solution for practical implementations.

Future explorations may consider additional optimizations and parameter adjustments to further bolster the control system's efficacy. It would be beneficial to conduct experimental validations on tangible EV platforms to corroborate the effectiveness of the proposed strategy. Extending this methodology to diverse control targets and

system configurations may pave the way for addressing varied EV control conundrums, aiming to elevate the overall system operation.

Data Availability

The data used to support the findings of this study are available from the corresponding author upon request.

Acknowledgements

The DG RSDT (Direction Générale de la Recherche Scientifique et du Développement Technologique) provided support for this work.

Conflicts of Interest

The authors declare that they have no conflicts of interest.

References

[1] K. Saidi, A. Boumediene, and D. Boubekeur, "An optimal ga-based backstepping control scheme for a mimo nonlinear system," *J. Eur. Syst. Autom.*, vol. 56, no. 1, pp. 89–96, 2023. https://doi.org/10.18280/jesa.560112

[2] I. Khalil, J. Doyle, and K. Glover, *Robust and Optimal Control*. Prentice Hall, 1996.

[3] G. Duc and S. Font, *Commande H∞ et μ-analyse : des outils pour la robustesse*. Paris: Hermes Sciences Publications, 1999.

[4] S. Skogestad and I. Postlethwaite, *Multivariable Feedback Control: Analysis and Design*. Hoboken, NJ, USA: John Wiley & Sons, 1999.

[5] K. Zhou and J. Doyle, *Essentials of Robust Control (Vol. 104)*. Upper Saddle River, NJ, USA: Prentice Hall, 1998.

[6] D. Gu, P. Petkov, and M. Konstantinov, *Robust Control Design with MATLAB®*. Springer Science & Business Media, 2005.

[7] K. Glover and J. C. Doyle, "State-space formulae for all stabilizing controllers that satisfy an h∞-norm bound and relations to risk sensitivity," *Syst. Control Lett.*, vol. 11, no. 3, pp. 167–172, 1988. https://doi.org/10.1016/0167-6911(88)90055-2

[8] J. C. Doyle, K. Glover, P. Khargonekar, and B. Francis, "State-space solutions to standard h2 and h ∞ control problems," *IEEE Trans. Autom. Control*, vol. 34, no. 8, pp. 831–847, 1989. https://doi.org/10.1109/9.29425

[9] C. Mi and M. Masrur, *Hybrid Electric Vehicles: Principles and Applications with Practical Perspectives*. John Wiley & Sons, 2017.

[10] E. Schaltz and S. Soylu, "Electrical vehicle design and modeling," *Electr. Veh.-Model. Simul.*, vol. 1, pp. 1–24, 2011. http://doi.org/10.5772/20271

[11] S. Boyd, L. El Ghaoui, E. Feron, and V. Balakrishnan, *Linear Matrix Inequalities in System and Control Theory*. Society for Industrial and Applied Mathematics, 1994.

[12] J. Buerger and J. Anderson, "Robust control for electric vehicle powertrains," *Control Theory Technol.*, vol. 17, pp. 382–392, 2019. https://doi.org/10.1007/s11768-019-8279-2

[13] T. Gillespie, *Fundamentals of Vehicle Dynamics*. Warrendale, PA, USA: Society of Automotive Engineers Inc., 1992.

[14] F. A. Salem, "Modeling and control solutions for electric vehicles," *Eur. Sci. J.*, vol. 9, no. 15, pp. 221–240, 2013.

[15] M. A. Shamseldin, "Design of auto-tuning nonlinear pid tracking speed control for electric vehicle with uncertainty consideration," *World Electr. Veh. J.*, vol. 14, no. 4, p. 78, 2023. https://doi.org/10.3390/wevj14040078

[16] S. Kim, J. S. Bang, S. Kim, and H. Lee, "Robust vehicle speed control using disturbance observer in hybrid electric vehicles," *Int. J. Autom. Technol.*, vol. 21, pp. 931–942, 2020. https://doi.org/10.1007/s12239-020-0089-5

[17] O. Kraa, M. Becherif, A. Aboubou, M. Y. Ayad, I. Tegani, and A. Haddi, "Modeling and fuzzy logic control of electrical vehicle with an adaptive operation mode," in *4th International Conference on Power Engineering, Energy and Electrical Drives*, Istanbul, Turkey, 2013, pp. 120–127. https://doi.org/10.1109/PowerEng.2013.6635592

[18] O. Kraa, M. Becherif, M. Y. Ayad, R. Saadi, M. Bahri, A. Aboubou, and H. Ghodbane, "States feedback control applied to the electric vehicle," *Energy Procedia*, vol. 50, pp. 186–193, 2014. https://doi.org/10.1016/j.egypro.2014.06.023

[19] R. K. Sharma, V. Sanadhya, L. Behera, and S. Bhattacharya, "Vector control of a permanent magnet synchronous motor," in *2008 Annual IEEE India Conference*, Kanpur, India, 2008, pp. 81–86. https://doi.org/10.1109/INDCON.2008.4768805

[20] S. Li, T. A. Haskew, and Y. K. Hong, "Characteristic study of vector-controlled permanent magnet synchronous motor in electric drive vehicles," in *IEEE PES Transmission and Distribution Conference and Exposition*, Orlando, Florida, USA, 2012, pp. 1–8. https://doi.org/10.1109/TDC.2012.6281468

[21] T. D. Do, H. H. Choi, and J.-W. Jung, "SDRE-based near optimal control system design for PM synchronous motor," *IEEE Trans. Ind. Electron.*, vol. 59, no. 11, pp. 4063–4074, 2012. https://doi.org/10.1109/TIE.2011.2174540

[22] J. Zhang, Q. Fan, M. Wang, B. Zhang, and Y. Chen, "Robust speed tracking control for future electric vehicles under network-induced delay and road slope variation," *Sensors*, vol. 22, no. 5, p. 1787, 2022. https://doi.org/10.3390/s22051787

[23] X. Jin, Q. Wang, Z. Yan, and H. Yang, "Nonlinear robust control of trajectory-following for autonomous ground electric vehicles with active front steering system," *AIMS Math*, vol. 8, no. 5, pp. 11 151–11 179, 2023. http://doi.org/10.3934/math.2023565

[24] P. Gahinet and P. Apkarian, "A linear matrix inequality approach to h∞ control," *Int. J. Robust Nonlinear Control*, vol. 4, no. 4, pp. 421–448, 1994. https://doi.org/10.1002/rnc.4590040403

[25] J. Baillieul and T. Samad, *Encyclopedia of Systems and Control*. Cham: Springer International Publishing, 2021. https://doi.org/10.1007/978-3-030-44184-5_300014

[26] P. Gahinet, "Explicit controller formulas for lmi-based h∞ synthesis," *Automatica*, vol. 32, no. 7, pp. 1007–1014, 1996. https://doi.org/10.1016/0005-1098(96)00033-7

[27] M. Ibrahim, M. Ibrahim, and S. Khather, "Design of fuzzy-ACO based controller for Cuk converter in electric vehicles," *J. Eur. Syst. Autom.*, vol. 56, no. 3, pp. 425–430, 2023. https://doi.org/10.18280/jesa.560309

[28] M. Attia, F. Zaamouche, A. Houam, and R. Daouadi, "Stability control modeling and simulation strategy for an electric vehicle using two separate wheel drives," *Eur. J. Electr. Eng.*, pp. 239–245, 2022. https://doi.org/10.18280/ejee.245-602

Nomenclature

EV	Electric Vehicle
$PMSM$	Permanent Magnet Synchronous Motor
$NEDC$	New European Driving Cycle
LMI	Linear Matrix Inequalities